June 2017

Laser Machining and Near Field Microwave Microscopy of Silver Inks for 3D Printable RF Devices

Anthony J. Ross III
University of South Florida, anthonyross@mail.usf.edu

Laser Machining and Near Field Microwave Microscopy of Silver Inks for 3D Printable RF Devices

by

Anthony J. Ross III

A thesis submitted in partial fulfillment
of the requirements for the degree of
Master of Science in Electrical Engineering
Department of Electrical Engineering
College of Engineering
University of South Florida

Major Professor: Thomas M. Weller, Ph.D.
Andrew Hoff, Ph.D.
Jing Wang, Ph.D.

Date of Approval:
June 13, 2017

Keywords: Additive Manufacturing, Microwave Filters, NFMM,
Fused Deposition Modeling, Square Open Loop Resonator

Acknowledgements

I want to take a moment to first acknowledge everyone in my life that has helped me along this path. I would first like to thank Dr. Thomas Weller for being an exemplary professor and advisor. I have truly learned a lot from you, and have been an incredible inspiration to me. Thank you to my committee members Dr. Andrew Hoff and Dr. Jing Wang, my parents Tony and Terry Ross for your encouragement and wisdom, last but not least Dr. Virginia Morgan and Alexander Ross for being by side and supporting me through this process.

Table of Contents

List of Tables

List of Figures

Abstract

3D printable materials for RF devices need improvement in order to satisfy the demand for higher frequency and lower loss performance. Characterization of materials that have shown improvements of conductor conductivity have been performed. By using a laser machining technique the loss of a 3D printed 2.45 GHz microstrip Square Open Loop Resonator (SOLR) bandpass filter has been shown to improve by 2.1dB, along with an increase in bandwidth from 10% to 12.7% when compared to a SOLR filter that has not been laser machined. Both laser machined and microwaved silver inks have been mapped for conductivity using a Near Field Microwave Microscope (NFMM) and have shown improvement of conductivity compared to inks that have been cured using standard methods.

Chapter 1 : Introduction

The arena of Additive Manufacturing (AM) has exploded in the last decade. It is now common place to find 3D printers everywhere that you go. A 3D printer can be purchased for an affordable price, and even conveniently located in a home to have the ability to design, print, and test in just a matter of hours. In the field of RF engineering specifically it allows a tremendous amount of design flexibility, as being able to print in three dimensions has allowed unlimited design configuration. While the use of 3D printing for RF devices has been expanding, the availability of printable materials on the other hand has seen less growth. The work of this thesis is to improve the conductivity of RF devices by different methods, and to characterize the materials using a near field microwave microscope (NFMM).

Much work has already been accomplished in 3D printing electronic and RF devices. Demonstrated devices include electronic circuits [1], sensors [2], antennas [3], filters [4], and complete RF front end systems [5].

There have been many issues that have been associated with 3D printing up until this point that need to be improved:

1. Poor conductivity of the 3D printed metallic layers
2. Surface roughness due to the substrate printing
3. Poor printable dielectric constant to be used as the substrate and supporting layers

Improvements in these areas will drastically improve the abilities of 3D printed devices by making them smaller and more lightweight as well as increasing the frequency in which we are

capable of operating. Poor conductivity directly affects the attenuation of the signal which leads to loss.

$$\sigma = \frac{1}{\rho} = \frac{1}{R_s * t} \tag{1}$$

$$\delta_s = \frac{1}{\alpha} = \sqrt{\frac{1}{\pi f \mu_0 \sigma}} \tag{2}$$

σ – DC Conductivity (S/m)
ρ – Resistivity (Ω-m)
R_s – Sheet Resistance (Ω/square)
α – Attenuation constant (Nepers/m)
δ_s – Skin Depth (m)

The main goal of this work is to study and characterize the effects of different methods of improving 3D printed materials in order to make them better for higher frequency applications. Chapter 2 goes over the 3D printing techniques that were used for this research. Chapter 3 goes over a SOLR filter that was fabricated using laser machining in order to improve the loss. The design, fabrication, testing, simulation, and NFMM results of the SOLR filter are discussed as well as a simulation to determine how much change in the loss results from the bandwidth increase. Appendix A reviews the NFMM system used in this research, and Appendix B discusses measurements from an experiment conducted in order to review the effect that microwave sintering has on the silver ink conductivity.

Chapter 2 : Additive Manufacturing Methods and Laser Sintering

Several different types of 3D printing methods are available. Some common printing methods include Fused Deposition Modeling, Powder Bed Fusion, and Stereolithography [6]. Each of them has its own advantages and disadvantages. AM when compared to subtractive manufacturing has less waste, therefore decreasing the cost. The two methods of 3D printing used in this research include FDM for the thermoplastic substrates, and micro dispensing for the conductive traces. This chapter will cover how these two methods work.

2.1 Fused Deposition Modeling

One of the most widely used methods for AM include Fused Deposition Modeling (FDM) which involves taking a plastic filament and running it through a heated nozzle until the material turns into a liquid, and then depositing the plastic onto the surface as the nozzle is scanned back and forth until one layer has been printed. The Z axis moves up a step in height and the next layer is printed directly on top of the first layer. This is done one layer at a time repeatedly until the entire part has been printed as shown in Figure 2.1. The nScrypt 3Dn printer that was used for this research has 3 motorized stages to allow for movement in the X, Y, and Z planes. For this system the accuracy in movement in the X, Y and Z planes is 0.5 μm.

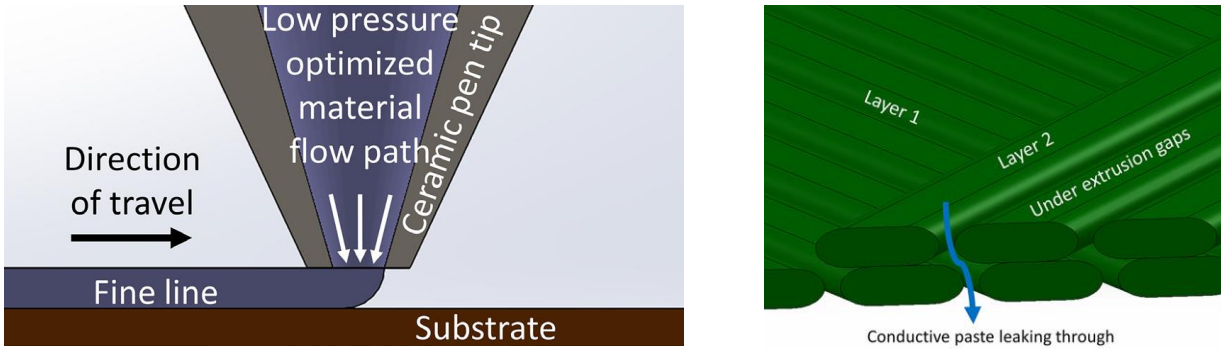

Figure 2.1 Image of FDM printing layer by layer [7] © 2017 IEEE

A 3D CAD file is first designed for the structure that is to be printed in programs such as SolidWorks or Inventor and then it is exported into a STL file format which describes the surface geometry of the part that has been printed. The STL file is then imported into a g-code generator program which takes the STL file along with any print variables that are specific to the print and material being used to export the code that will be used in manufacturing the part. Some examples of variables used in the process include the speed of the print, speed of material feed, width of print line, nozzle size and many more. These define the print and are typically changed depending upon the material used during the print.

Parts may also be printed with varying levels of infill. This defines that amount of material that is being used on the inside of the printed part. Printing with 100% infill is not necessary for many applications. Time and money can be saved if less material is used during the printing process. Depending upon the infill percentage that is used, both the mechanical and electrical properties of the material can change. In a typical 3D printed RF design 100% infill is used, but if needed the mechanical and electrical properties of the printed material can be tuned by changing the infill [8], [9]. An example of different percentages of infill can be seen in Figure 2.2.

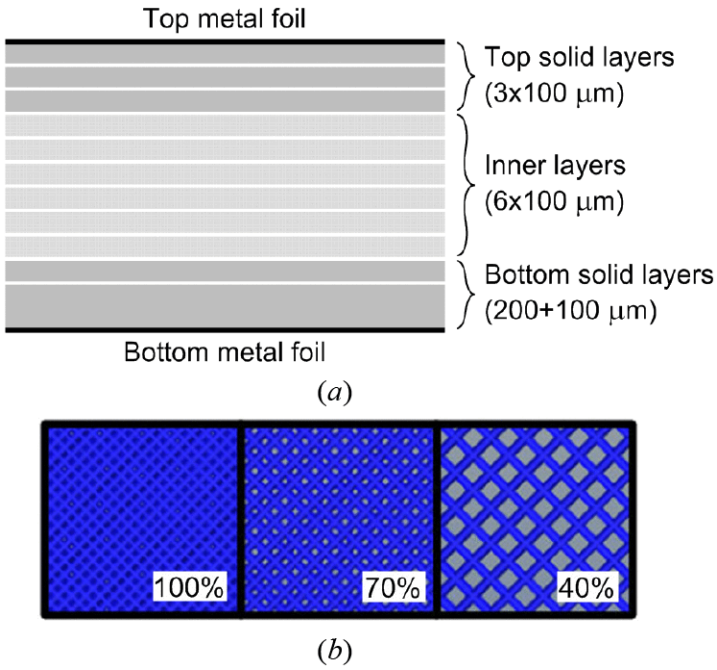

Figure 2.2 Infill of inner layers for a typical 3D print [8] © 2016 IEEE

Some of the main advantages to using FDM printing include the affordability of the printer and the wide range of materials that are available. Some of the disadvantages that FDM has include the slow build speed, accuracy of the print, and material density [6]. For instance a layer that is 0.145 μm thick is not possible because the printer cannot move its axis to that small of a dimension. Density is also not comparable to other manufacturing methods such as injection molding. During printing unwanted air gaps tend to leave lower densities which can be a significant issue for RF devices. In order to improve the print so that this does not occur the raster gap can be decreased during the print in order to get to higher densities [10]. Higher material density will lead to more accurate and consistent substrate dielectric constant.

2.2 Micro Dispensing Conductive Inks

For printing conductive traces there are several widely used methods available including FDM, aerosol jetting, and microdispensing. Many manufactures sell conductive filaments that can be printed using an FDM system. Although this method is easy to print, the disadvantage is that

most available conductive filaments have high resistances that do not make it feasible to be used for signal traces. Aerosol jet is a popular method for depositing metal lines. This process involves using a gas to push the inks in order to be deposited as a mist. Fine lines as small as 5μm can be realized using this method. Microdispensing is another technique that is widely used for depositing metals. It is simple to use and an inexpensive technique that involves forcing an ink directly through a nozzle to the surface. For the rest of this section this technique will be reviewed in detail.

In order to microdispense silver ink accurately offsets in the print design need to be accounted for prior to printing. The spreading of the ink depends upon the viscosity and can change for different inks, and different temperatures. If it is not accounted for print widths can be much different than expected. The first step is to do a test print of a single line at the speed and temperature in which the design will be printed. This will determine the overall width of the printed line. For instance when using a 150 μm tip the ink printing width will be ~200 μm due to spreading. Offsets in the design will need to be accounted for high accuracy.

The file can be uploaded into a CAD software like AutoCAD in raw format shown in Figure 2.3a, then offset to the inside of the design ~100 μm which is half the width of the print twice shown in Figure 2.3b. Since the print width of the tip is ~200 μm offsetting the design allows the spreading to be accounted for. The outside design can then be removed, and the inside design can be used to create the rastering (Figure 2.3c) for the interior print to minimize spreading due to excessive ink being printed. This final design is then converted into a program that will be used to create the movement commands that will be sent to the motors and ink pump in order to create the desired printed surface. PCAD from nScrypt was the software used in this research.

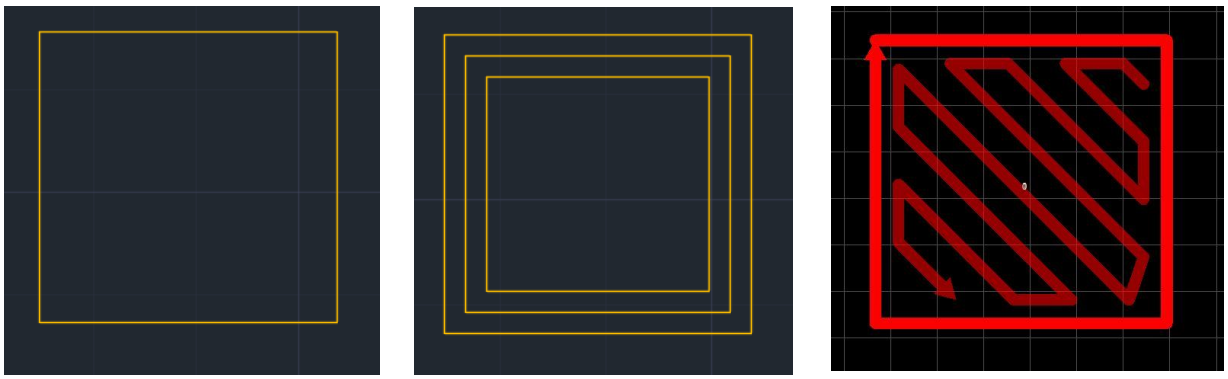

a) b) c)

Figure 2.3 Formation of lines for silver ink printing

The inks used in microdispensing are thick film pastes having metal micro sized particles along the size of 10μm or less embedded in a polymer matrix. For microdispensing the rule of thumb for deciding the nozzle size to be used for printing in order to keep from clogging is to make sure that the inner diameter of the pen tip is at least 10 times bigger than that of the particle size [7]. After the ink is printed it is oven baked in order to remove the solvents. The higher the temperature and the longer the bake used determines the ending conductivity of the ink once dried.

Some issues that tend to arise during the microdispensing of inks include lower conductivity, surface roughness, non-uniform particles, and inaccurate printing dimensions from ink spreading. Particulates settle in the matrix non-uniformly toward the bottom of the signal trace as the ink dries causing the effective RF conductivity to vary from ~0.6e6 S/m to ~2e6 S/m which has an undesired effect on attenuation [11]. Shown in Figure 2.4 is a cross section SEM image of printed CB028 ink. Also due to roughness of the surface there is an added difficulty in printing precise dimensions due to ink flowing with varying viscosities due to differences in temperature. The surface roughness of the material helps the ink to spread to quickly causing dimensions to be different than the original design varying in both length and thickness.

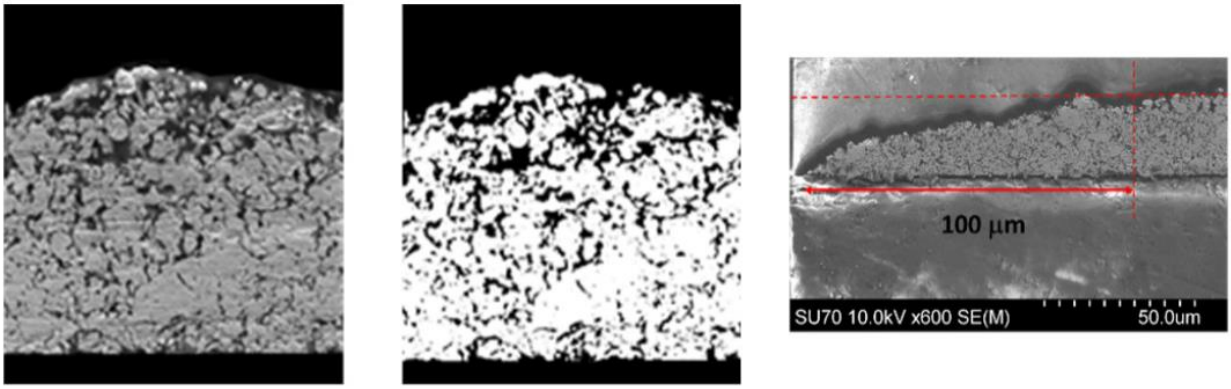

Figure 2.4 Cross section SEM images of CB028 trace [7] © 2017 IEEE

The ink of choice for this research is Dupont CB028 [12] which was deposited using the microdispensing technique on an nScrypt 3Dn printer with a Smart Pump™ head. Typical thickness of the ink once printed is in the range of 25 µm. Oven baking the ink once printed. For the prints done in this research, baking was performed for 1 hr at 90°C. The longer the baking and the higher the temperature the conductivity of the ink increases. The heat deflection temperature of the substrate is a critical factor in determining the maximum temperature the substrate can be baked in order to not cause damage [5]. Varying heat deflection temperatures (HDT) depending upon the printed substrate, and typical baking temperatures with subsequent trace conductivities can be found in Table 2.1 and Table 2.2.

Table 2.1 Heat Deflection Temperature (HDT) of FDM compatible materials [5] © 2015 IEEE

Material	Dielectric constant	Loss tangent	Glass transition temp *Tg* (°C)	Heat deflection temp (HDT) @ 1.8 MPa (°C)
PLA	3.1	0.010	65	43
ABS	2.6	0.0078	105	88
COP	2.12	0.0009	135†	134
30 vol.% COP-TiO_2	4.57	0.0014	110†	
PC	2.8	0.005	147	128-138
ULTEM™	2.27	0.0121	200†	153

Table 2.2 Bulk DC conductivity of CB028 silver paste [5] © 2015 IEEE

Cure temperature	Conductivity (S/m)	Compatible material
60°C	1.75e6	PLA
90°C	2.62e6	ABS
130°C	3.94e6	PC
160°C	4.63e6	ULTEM™

2.3 Laser Sintering

Laser sintering of conductive ink is the act of using a laser in order to change the particles of the ink in such a manner that they go more from a micro particle form into a solid. The laser is used to heat up the porous particles in such a manner that the material compresses and becomes more solid, thus producing a more uniform material. Compared to baking the ink it takes much less time and drastically decreases the electrical resistivity of the ink compared to baking alone. Since substrates being printed upon have limitations in temperature, laser machining is a much better option comparatively in terms of time and temperature limitations [13].

Chapter 3 : SOLR Filter Laser Treatments to Improve Conductivity

Square open loop resonator (SOLR) filters are frequently used in communication systems due to their small size, narrow bandwidth, low insertion loss and high selectivity [14]. For this study SOLR bandpass filters were fabricated using additive manufacturing techniques and an in situ laser to machine the gap between the resonators with different widths to demonstrate the improvement of insertion loss of the filter using this technique. The laser machined filter shows 2.1 dB reduction in the insertion loss compared to a comparable non-machined filter topology, although the increased bandwidth also accounts for some of the loss improvement.

3.1 Laser Machining

Printing silver ink directly on top of ABS substrates has its challenges. There are limitations as to the dimensions that can be printed with silver ink accurately depending upon the roughness of the printing surface. Spreading of ink on the surface before it has had enough time to dry can cause undesired effects including non-uniform edges or shorting when printing small features. Due to these effects a 3D printer is only capable of reliably printing gaps of ~240 μm on an ABS surface made using fused deposition modeling, without any issues affecting the print and the outcome of the fabricated design. In order to solve this issue an in situ laser is used in conjunction with the ink printing in order to facilitate designs that need features to be smaller than 240 μm. One cut with the laser can yield a reliable feature size that is as small as 16 μm in width, and can be scaled up to any size when multiple cuts are done side by side.

Shown in Figure 3.1 is a comparison of 3D printing lines with and without laser machining. Normal printing tends to leave jagged edges due the roughness of the substrate, and laser machining tends to leave cleaner edges. The cleaner cut helps to decrease the odds of creating a short across gaps, allows smaller dimensions to be used in designs.

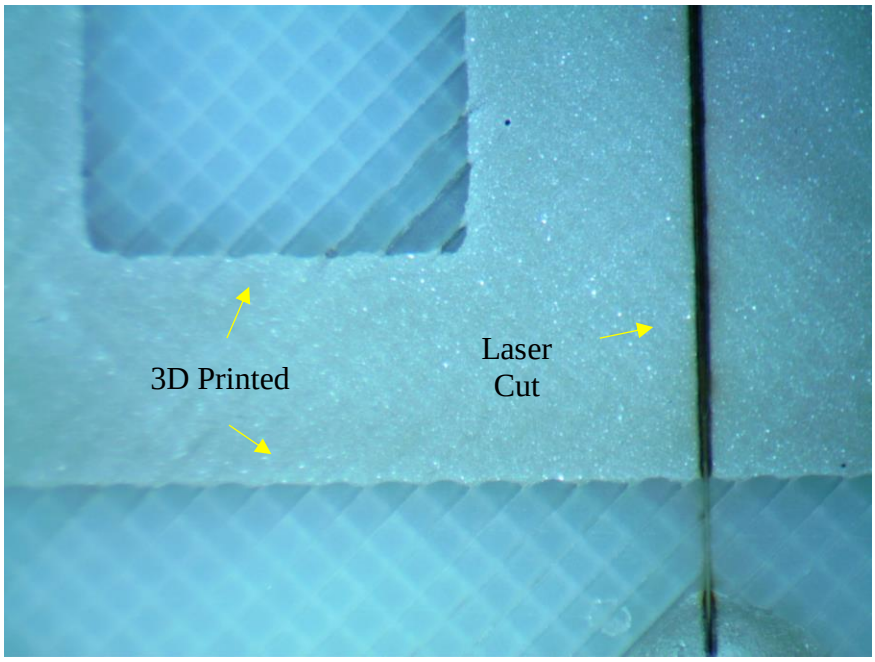

Figure 3.1 Printed features with and without laser machining

In previous work SOLR filters were designed and fabricated with the goal of minimizing the feature size of the 3D printed filter as well as decreasing the insertion loss [4]. Typical planar ink printing with a minimum gap size of 240 μm was compared to a filter that was printed with an overlay capacitor that bridges the gap as an alternate solution, and it was found that the IL could be decreased even further by adding the overlay capacitor.

Laser machining has also been previously shown to improve the conductivity of the ink near the edges of 3D printed coplanar waveguide transmission lines and filters with the improvement of the conductivity on the cut line increasing as much as 100 times to improve losses [15]. With improved conductivity lower loss RF circuits can be fabricated and higher frequency

designs with improved performance can be realized. A SEM image of laser machined ink is shown in Figure 3.2.

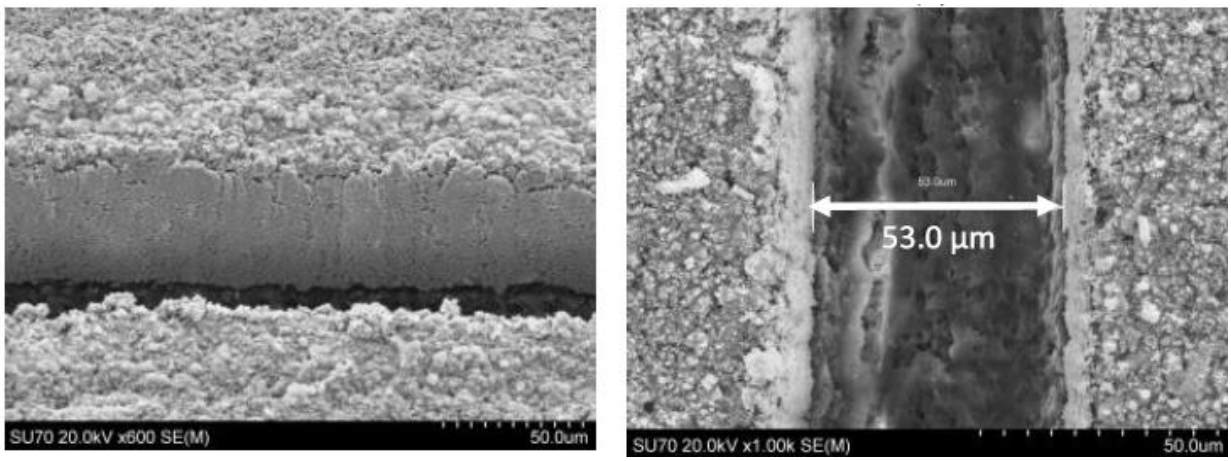

Figure 3.2 SEM images of laser machined lines [15] © 2017 IEEE

3.2 Fabrication and Testing of a Laser Machined SOLR Filter

Two SOLR bandpass filters were fabricated using 3D printing and laser machining combined. One filter has a 240 µm gap using 3D printing alone, and a second SOLR filter that was fabricated using the laser to machine a 16 µm gap. The device was printed using an nScrypt 3Dn printer with ABS and Dupont CB028 ink. Several layers of ABS and ink were printed. The first layer of ABS was printed as a structural support followed by the ground plane, ABS microstrip substrate, and signal layer. The ABS was printed at a temperature of 280° C with the chuck temperature held at 90° C. An Nd: YAG Lumera laser was used to laser machine the resonator gaps with the power setting at 0.75 W with 10 passes at a speed of 25 mm/s. Following the printing the filter was baked in an oven at 90° C for an hour in order to dry the ink and improve the conductivity. Shown in Figure 3.3 are the cross section and top view of the device.

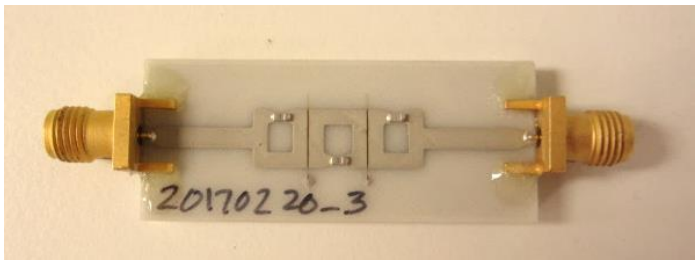

a)

b)

Figure 3.3 SOLR laser machined filter a.) Top view b.) Cross section

The design of the SOLR filter is a 3 section resonator filter with 0.7 pF coupling capacitors added in order to assist in helping to decrease the design size [16]. Shown in Table 3.1 and Figure 3.4 are the dimensions of the filter.

Table 3.1 Post printing parameters for 16 μm SOLR filter

Parameter	**Value**
ABS substrate height	30 mils (0.762 mm)
DC Conductivity of ink (Baked)	2.62 MS/m
Ink thickness	25 μm
Gap thickness	16 μm

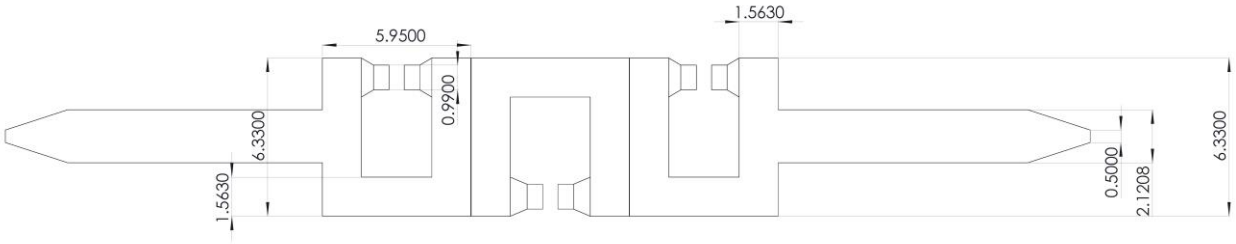

Figure 3.4 Dimensions of SOLR filter with a 16um gap

S_{21} and S_{11} parameters of the two SOLR filters were measured using a Keysight E5063A VNA. Measured results of the SOLR filters are shown in Figure 3.5. The insertion loss (IL) of the 16 μm gap filter shows a decrease from 4.8 dB to 2.7 dB and the bandwidth (BW) has increased from 10.7% to 12.7% when compared to the filter with the 240 μm gap.

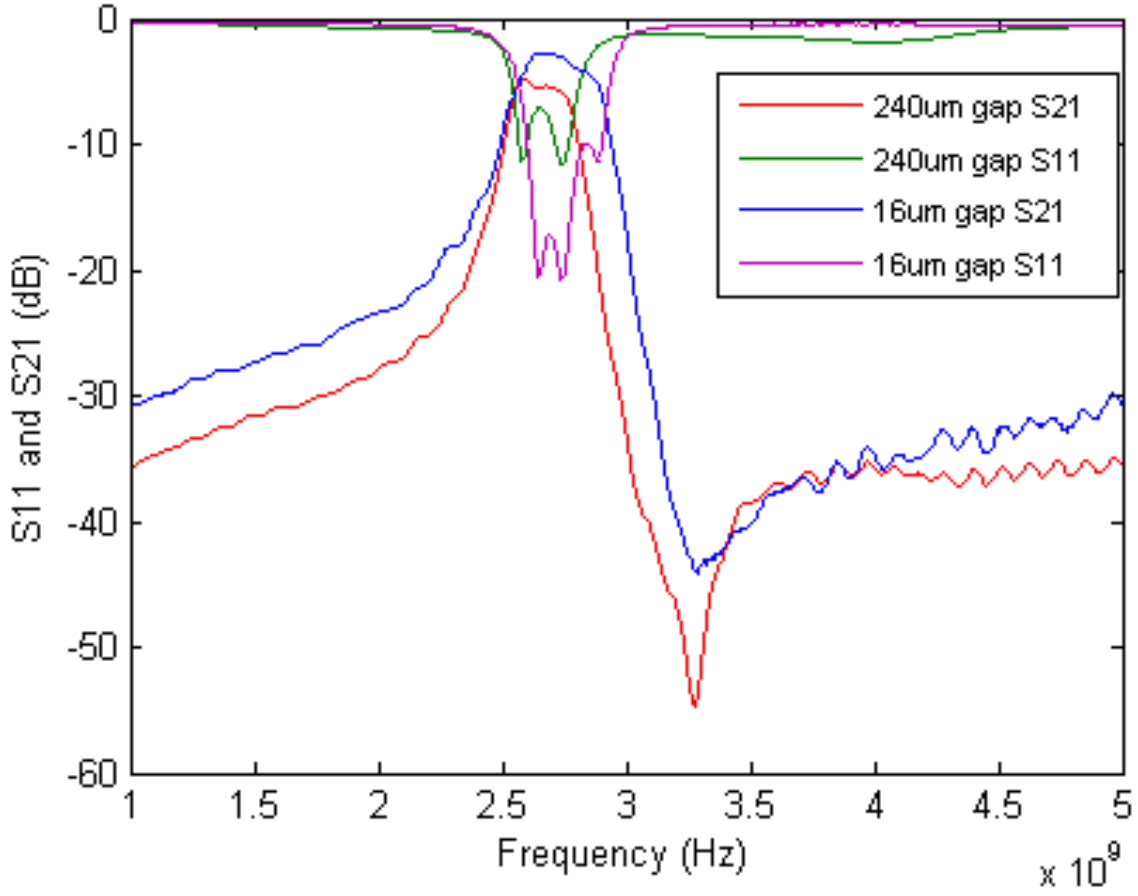

Figure 3.5 Comparison of 240 μm and 16 μm gap SOLR filters

Simulated and measured results of the 16 μm gap filter are shown in Figure 3.7. The simulation was performed using Ansys HFSS, then S Parameters were exported into Keysight ADS. The three 0.7pF ATC 0603 series surface mount capacitors from the Modelithics library were then added in order to get the final simulation. Microstrip parameters used in the simulation include $\varepsilon_r = 2.6$, $\tan\delta = 0.007$, T = 25 μm, H = 30 mils, $\sigma_{gapedge} = 5$ MS/m, $\sigma_{plane} = 2.62$ MS/m. The

conductivity near the gap of the laser machined region was measured using a NFMM and was found to be ~5 MS/m. The results from NFMM are described in Section 3.4. Simulations in HFSS were performed with 2 different conductivity regions shown in Figure 3.6 which shows a close up of the two planes to take into account the laser machined edge. σ_{plane} is used for the entire trace except for the 4 μm near the edge of the gap on both sides which is simulated with $\sigma_{gapedge}$.

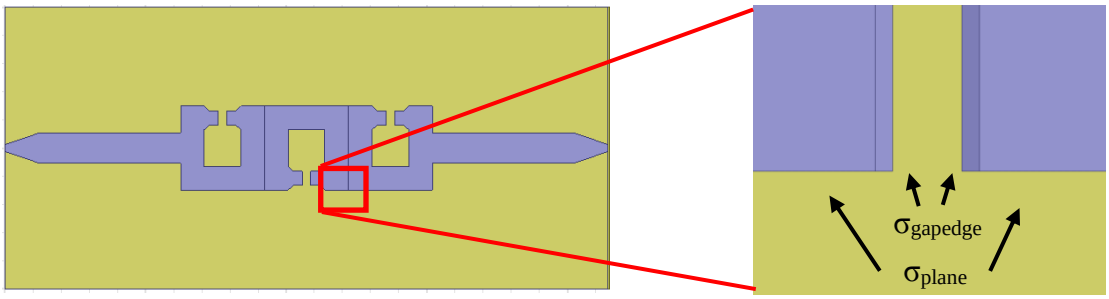

Figure 3.6 Gap top view of σ_{plane} and $\sigma_{gapedge}$ (4 μm wide) conductivity regions used in simulation

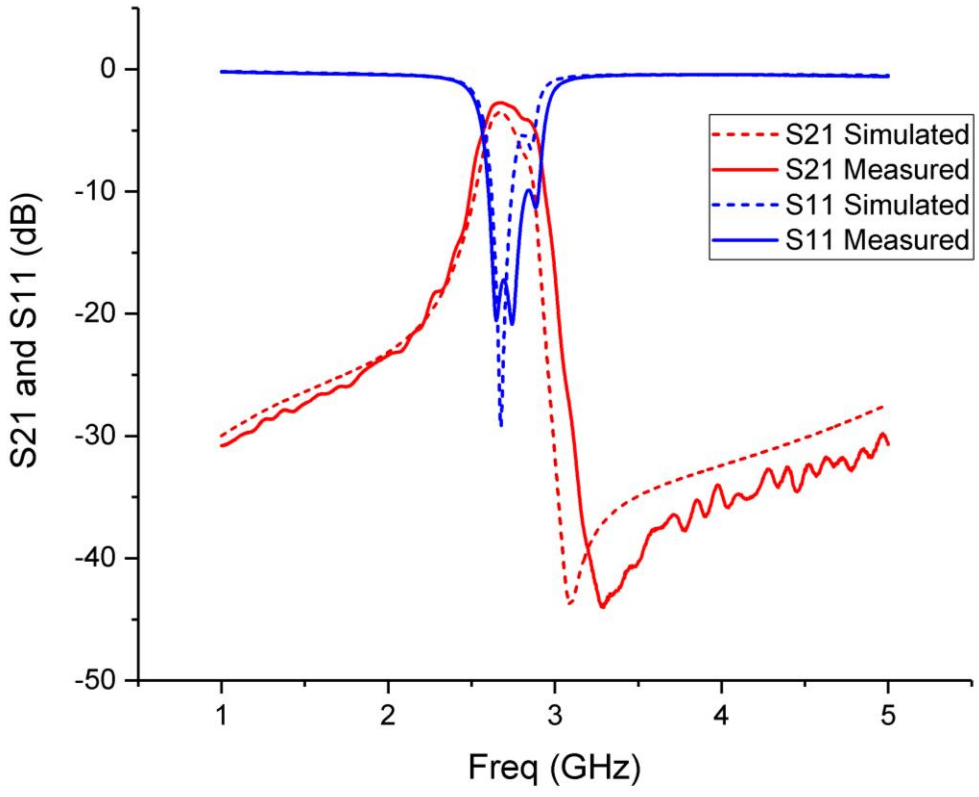

Figure 3.7 Simulated and measured S-parameters for the 16 μm gap SOLR filter

When compared to the results of two previously fabricated SOLR filters the filter that has the gap between the resonators laser machined to a 16 μm width had the lowest measured insertion loss. Shown in Table 3.2 is a complete listing of results from 3D printed filters in a previous study compared to the 2 filters that were printed in this study. Filter 3 was 3D printed normally, and filter 4 was printed with overlay capacitors that spanned across the gaps. The insertion loss of the 16 μm gap filter is much lower by comparison. Several factors attribute to the decrease in loss including the increase in bandwidth by the gap being smaller as well as the higher conductivity near the edges of the gaps due to the laser machining. In Table 3.2 Gap is the distance between the resonators, C is the size of the capacitor used to load the resonator in order to help decrease the size [16], and IL is the measured insertion loss.

Table 3.2 Parameters for filters

Filter	**Gap (μm)**	**C (pF)**	**IL (dB)**	**BW (%)**	**Ref**
Filter 1	240	0.7	4.8	10.7	This work
Filter 2	16	0.7	2.7	12.5	This work
Filter 3	240	0.5	4.1	9.4	[5]
Filter 4 – Coupling Cap	500	0.7	3.8	10.2	[5]

3.3 NFMM Measurements

In order to determine the true conductivity of the laser machined gaps of the SOLR filters after fabrication a NFMM was used to create an image of both conductivity as well as height. Industry standard measurements such as Van der Pauw and 4-point probe methods are not available for the measurement due to the small size of the gap. These methods can only be used in order to determine the bulk resistivity of the material, but cannot measure material properties on the microscopic scale. A dielectric resonator (DR) NFMM probe was used for this work in order

to determine conductivity due to its fine sensitivity to conductive materials and micro-precision and allows for much finer control in measurements as well as surface mapping. Details describing the NFMM probe used for this research can be found in Appendix A.

Prior to measuring the silver ink of the filters a calibration was performed with several known conductive samples. The calibration standards from MTI Corporation listed on Table 3.3 were first scanned using the probe in order to determine the Q value at a height of 4 μm for each sample with known conductivities. An exponential equation was then obtained shown in Equation 1 which can be used to determine the conductivity for an unknown sample. Shown in Figure 3.8 is the plotted exponential fit along with the measured Q of the calibration standards. Each point on the curve was an average of 6 measurements.

Table 3.3 Dielectric resonator NFMM calibration material properties

Material	**Part Number**	**Size (mm3)**	**ρ (Ω*m)**	**σ (S/m)**
Ni	G1415	10x10x1	6.93E-08	1.44E+07
Ti	G140103	10x10x0.5	4.20E-07	2.38E+06
Stainless Steel	G14108	10x10x0.3	7.30E-07	1.37E+06

$$\sigma = 123.78e^{0.0198Q} \quad (3)$$

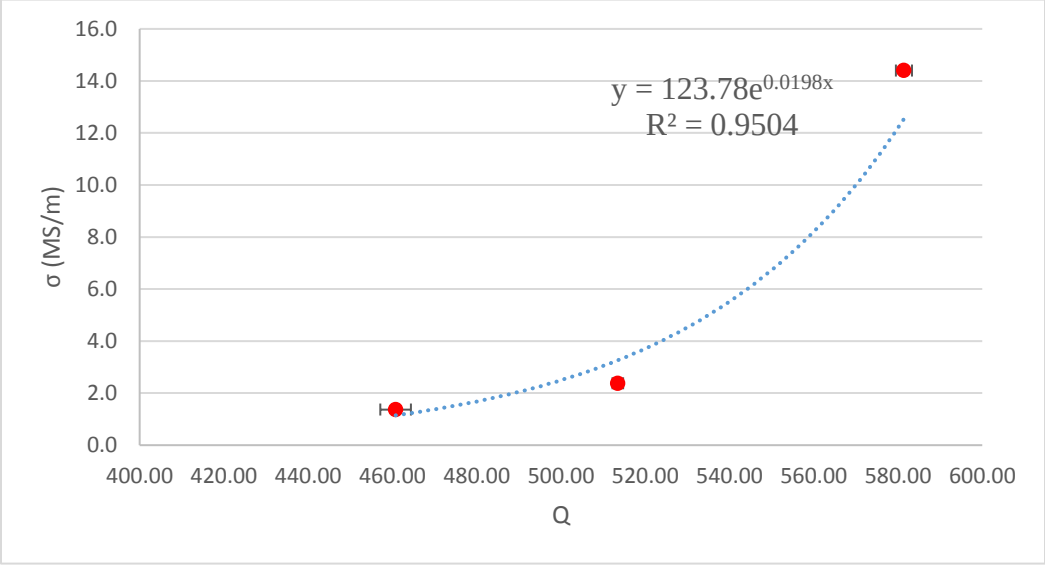

Figure 3.8 DR NFMM calibration curve for SOLR filter measurements

The NFMM was used to measure the conductivity of the ink directly on top of the gap edge and laser machined gap. The map in Figure 3.9 shows the silver ink on the bottom half of the image while the gap is located on the top. The gap in this image is a 240 μm wide cut in order to get a good image due to the radius of the probe tip is 25 μm. Conductivity measured near the edge of the ink close to the laser machined gap shows an average value of 4.32 MS/m with regions reaching a maximum value of ~5 MS/m.

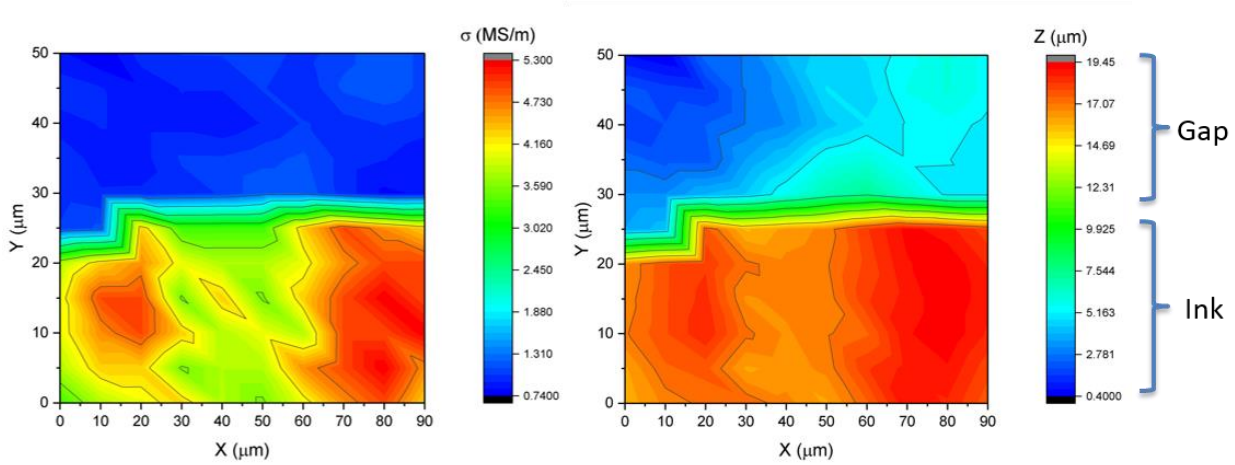

Figure 3.9 NFMM map of conductivity and height imaged along the edge of the laser machined gap

Conductivity was also measured in the middle of the trace is shown in Figure 3.10 with an average of 3.85 MS/m compared to the average measured along the edge of the gap of 4.32 MS/m shown in Figure 3.9. The NFMM measurement technique is only sensitive to the conductive metallic layers, so the conductivity data in measured in the center of the gap in Figure 3.9 can be disregarded since there is no metal in that region.

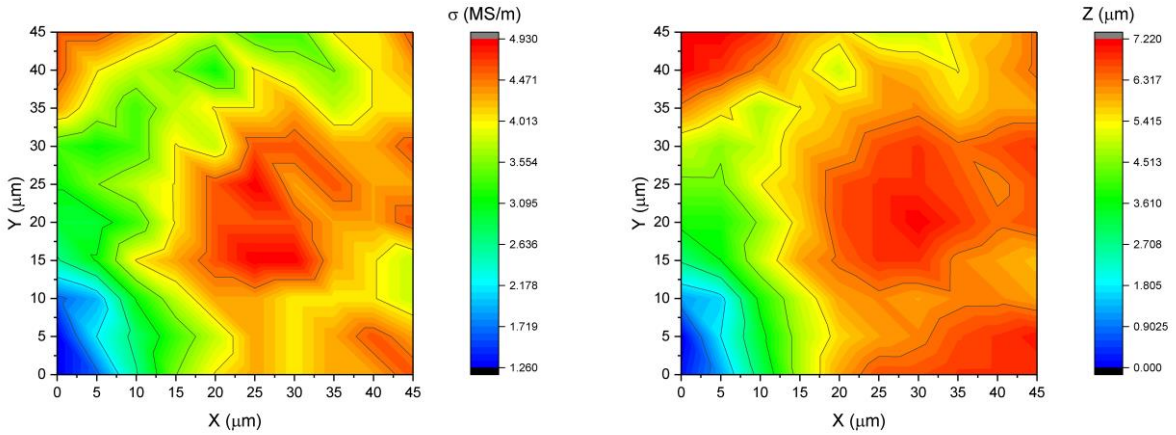

Figure 3.10 Conductivity and height map in middle of trace on SOLR filter

Another map of conductivity shown in Figure C.1 taken on a separate sample shows that the conductivity measured near the laser machined gaps is as high as 32 MS/m in spots which agrees close with the effective conductivity that was found in previous work where filters were fabricated by laser machining into ink [15]. If an SOLR filter were to be fabricated by laser machined along all edges of the filter rather than only between the gaps a similar increase in effective conductivity of the sample improve as well.

3.4 Coupled Line Filter Simulations

In order to determine why the loss improved as the bandwidth (BW) of the SOLR filters increased simulations of several coupled line filters were performed with varying BW. All coupled line filters were simulated with the same conductivity in order to demonstrate how the loss changes as the BW changes. As the bandwidth changes the loss is shown to improve as well, and this is shown to be independent upon the conductivity of the line.

Three first order coupled line filters centered at 1 GHz were designed using Keysight ADS with varying bandwidths from 5% to 30% with a 0.5 dB ripple Chebyshev response. Each filter was designed for the first order consisting of two microstrip coupled line segments, and two 50Ω microstrip line segments adjoining the coupled lines shown in Figure 3.11. Equations 4-10 were

used in order to determine the impedances of each line section [17]. First both the even and odd mode impedances were determined for each coupled line segment. Δ is the BW percentage defined by Equation 4 at the 3 dB points, f_h is the high frequency, f_l is the low frequency, and f_r is the resonant frequency, Z0Jn is the admittance inverter, Z0e is the even mode impedance, Z0o is the odd mode impedance.

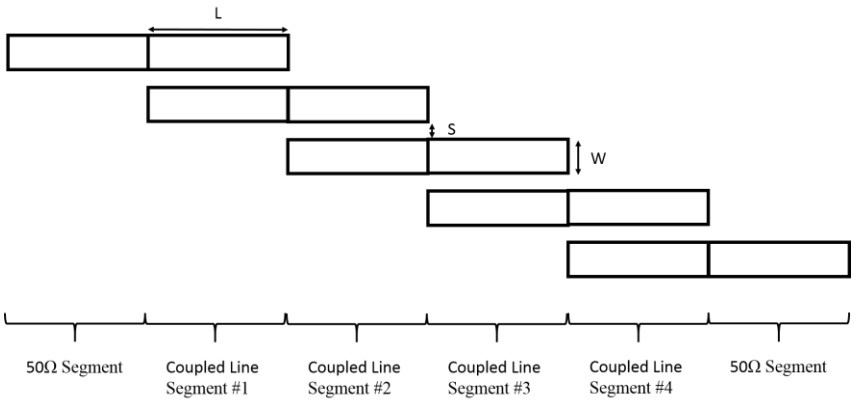

Figure 3.11 Coupled line filter design

$$Z_0 J_1 = \sqrt{\frac{\pi \Delta}{2 g_1}} \tag{4}$$

$$Z_0 J_n = \frac{\pi \Delta}{2\sqrt{g_{n-1} g_n}} \text{ for n = 2 and 3} \tag{5}$$

$$Z_0 J_4 = \sqrt{\frac{\pi \Delta}{2 g_3 g_4}} \tag{6}$$

$$\Delta = \frac{f_h - f_l}{f_r} \tag{7}$$

$$f_r = \sqrt{f_h * f_l} \tag{8}$$

$$Z_{0e} = Z_0(1 + JZ_0 + (JZ_0)^2) \tag{9}$$

$$Z_{0o} = Z_0(1 - JZ_0 + (JZ_0)^2) \tag{10}$$

The substrate and conductor used in the simulations is ABS and CB028. The ABS substrate has a relative dielectric constant of 2.6, tanδ of 0.007, height of 30 mils, trace thickness of 25 μm, and a trace conductivity of 2.62 MS/m. Dimensions needed for each coupled line segment were then determined using ADS Linecalc and are shown in Table 3.4. The adjacent 50 ohm line segments are 81.6 mils wide and 100 mils long.

Table 3.4 Design components of a third order coupled line filter

BW (%)	n	gn	Z0Jn	Z0e (Ω)	Z0o (Ω)	W (mils)	S (mils)	L (mils)
10.1	1	1.60	0.36	74.28	38.51	60.34	5.76	2075.69
	2	1.10	0.15	58.91	43.47	76.68	22.95	2032.55
	3	1.60	0.15	58.91	43.47	76.68	22.95	2032.55
	4	1.00	0.36	74.28	38.51	60.34	5.76	2075.69
11.6	1	1.60	0.38	76.59	38.17	58.03	5.10	2081.30
	2	1.10	0.18	60.49	42.68	75.15	18.69	2037.30
	3	1.60	0.18	60.49	42.68	75.15	18.69	2037.30
	4	1.00	0.38	76.59	38.17	58.03	5.10	2081.30
13.2	1	1.60	0.41	78.81	37.91	55.88	4.61	2086.48
	2	1.10	0.20	62.13	41.95	73.45	15.42	2042.24
	3	1.60	0.20	62.13	41.95	73.45	15.42	2042.24
	4	1.00	0.41	78.81	37.91	55.88	4.61	2086.48
13.9	1	1.60	0.42	79.90	37.81	54.87	4.40	2088.92
	2	1.10	0.21	62.97	41.60	72.55	14.07	2044.75
	3	1.60	0.21	62.97	41.60	72.55	14.07	2044.75
	4	1.00	0.42	79.90	37.81	54.87	4.40	2088.92

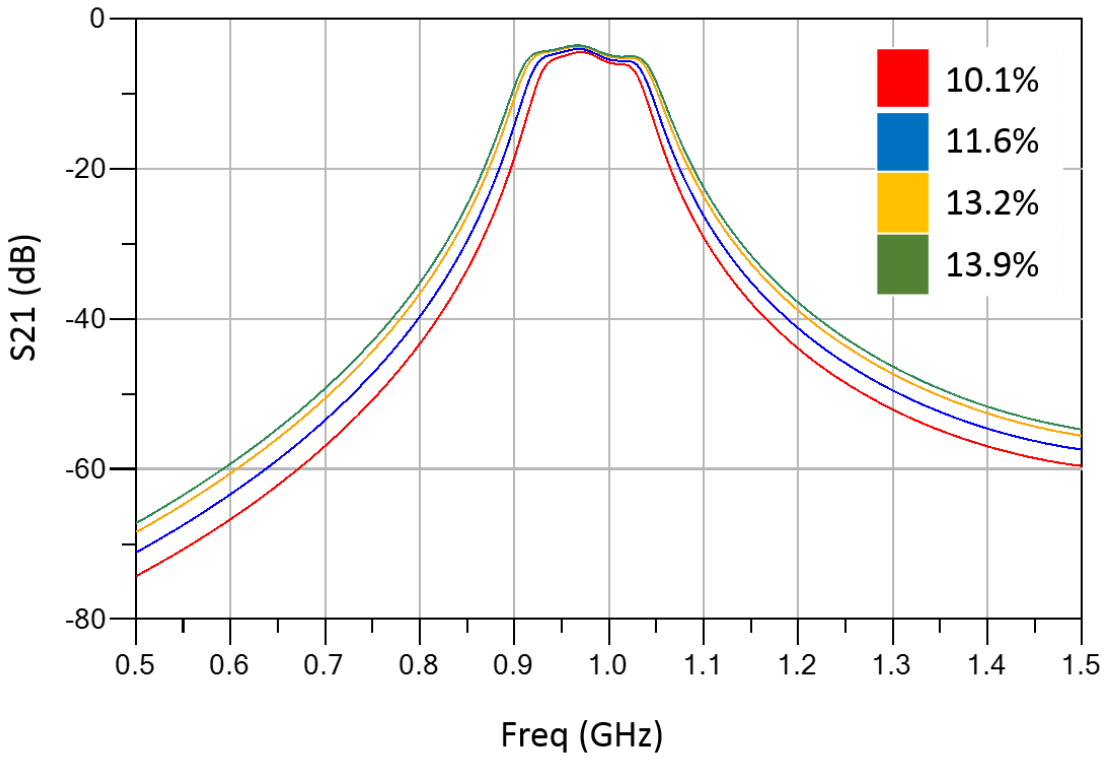

Figure 3.12 S21 of coupled line filters with varying bandwidths

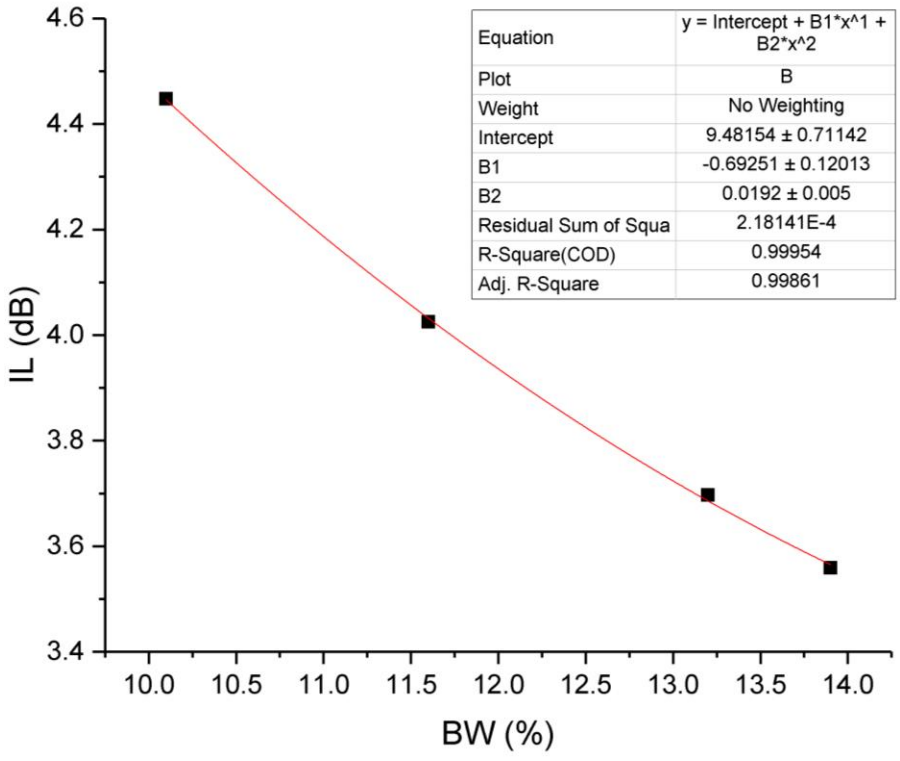

Figure 3.13 Coupled line filter BW vs IL

Shown in Figure 3.12, as the designed bandwidth of the filter is increased the insertion loss decreases. This is one of the factors contributing to the decrease in insertion loss of the laser machined SOLR filter. Bandwidth versus insertion loss is plotted in Figure 3.13, and based off of the simulated results a polynomial fit was found in order to estimate the change in loss. By adjusting the gap size of the SOLR filter from 240 μm to 16 μm a change in bandwidth from 10% to 12.7% has been measured. Comparing the change in bandwidth from the SOLR filter to the measured change in the coupled line filter simulations shows that a contribution of 0.69 dB out a 2.1 dB change can be accounted for from the change in bandwidth alone.

3.5 Conclusion

Several SOLR bandpass filters have been fabricated using both conventional 3D printing techniques and a new technique utilizing a laser to machine the gap in between the resonators. Compared to the filter printed using conventional methods, the filter with the laser machined 16 μm gap shows improvement of insertion loss by 2.1 dB and increase in bandwidth from 10% to 12.7% when compared to a filter fabricated with a 240 μm gap. An improvement of ~0.69 dB in insertion loss has been found to be due to the increase in BW. The IL measured on the 16 μm gap SOLR filter is 1.1 dB lower than in previous work [4]. A NFMM was used in order to measure the conductivity near the gap which measured close to 5 MS/m and as much as 32 MS/m on a separate sample.

Chapter 4 : Summary and Recommendations

Several SOLR filters were fabricated in order to improve the insertion loss and to be able to compare SOLR filters using both laser machining and standard 3D printing side by side. Another goal of this work was to gain a better understanding of how much the conductivity of the ink is changing when the ink is laser machined by using a NFMM to directly measure the conductivity near a laser machined gap. The IL of the SOLR filter with the laser machined gap had an improvement of 2.1 dB as well as a bandwidth increase from 10% to 12.7%. The improvement of IL from the change BW due to a smaller gap size alone shows a decrease of the loss of ~0.69 dB. The conductivity along the gap edge was measured to be 5 MS/m along the edge of the laser machined SOLR filter gap

Microdispensed silver inks were microwaved in order to improve the conductivity shown in Appendix A. Several different methods were used in order to determine the improvement. A four point probe measurement shows an increase of bulk conductivity from 1.74 MS/m to 8.51 MS/m by varying the microwaving time from 1 second to 60 seconds respectively. NFMM measurements of surface conductivity show a similar increasing trend in Q values which implies that there is an increase in conductivity. When the Q values measured are matched up to calibration data it shows that there is consistency between measured bulk conductivity data taken with the 4-point probe and surface conductivity measurements taken with the NFMM.

Recommendations for further work include:

1. Determining how much improvement of the overall insertion loss is due from the roughness decrease between the laser machined side walls when compared to non-laser machined edges.
2. Fabrication of SOLR filters by combining both laser machining techniques and COP/ceramic substrates. Prior work has shown that the COP/ceramic substrates have higher relative dielectric constants and lower tanδ. These two techniques combined will help to further decrease the size of the SOLR filters while continuing to improving the insertion loss.
3. Fabrication of a SOLR filter that has been machined along all edges in order to improve the effective conductivity.
4. Continued work in characterizing the microwaved silver inks. Measurements show good improvement in conductivity, but further investigations need to be made in order to develop a suitable process to be used with 3D printed RF devices.

References

[1] P. Deffenbaugh, "3D PRINTED ELECTROMAGNETIC TRANSMISSION AND ELECTRONIC STRUCTURES FABRICATED ON A SINGLE PLATFORM USING ADVANCED PROCESS INTEGRATION TECHNIQUES," *Thesis, UTEP, El Paso, TX*, 2014.

[2] T. Le *et al.*, "A novel strain sensor based on 3D printing technology and 3D antenna design," in *2015 IEEE 65th Electronic Components and Technology Conference (ECTC)*, 2015, pp. 981-986.

[3] J. M. O'Brien, J. E. Grandfield, G. Mumcu, and T. M. Weller, "Miniaturization of a Spiral Antenna Using Periodic Z-Plane Meandering," *IEEE Transactions on Antennas and Propagation*, vol. 63, no. 4, pp. 1843-1848, 2015.

[4] N. C. Arnal, "A Study on 2.45 GHz Bandpass Filters Fabricated With Additive Manufacturing," *Graduate Theses and Dissertations - USF*, 2015.

[5] T. P. Ketterl *et al.*, "A 2.45 GHz Phased Array Antenna Unit Cell Fabricated Using 3-D Multi-Layer Direct Digital Manufacturing," *IEEE Transactions on Microwave Theory and Techniques*, vol. 63, no. 12, pp. 4382-4394, 2015.

[6] I. Gibson, D. Rosen, and B. Stucker, "Additive Manufacturing Technologies 3D Printing, Rapid Prototyping, and Direct Digital Manufacturing," 2015.

[7] K. H. Church *et al.*, "Multimaterial and Multilayer Direct Digital Manufacturing of 3-D Structural Microwave Electronics," *Proceedings of the IEEE*, vol. 105, no. 4, pp. 688-701, 2017.

[8] S. Moscato *et al.*, "Infill-Dependent 3-D-Printed Material Based on NinjaFlex Filament for Antenna Applications," *IEEE Antennas and Wireless Propagation Letters*, vol. 15, pp. 1506-1509, 2016.

[9] L. Baich and G. Manogharan, "STUDY OF INFILL PRINT PARAMETERS ON MECHANICAL STRENGTH AND PRODUCTION COST-TIME OF 3D PRINTED ABS PARTS " *Solid Freeform Fabrication Symposium*, 2015.

[10] M. Dawoud, I. Taha, and S. J. Ebeid, "Mechanical behaviour of ABS: An experimental study using FDM and injection moulding techniques," *Journal of Manufacturing Processes*, vol. 21, pp. 39-45, 1// 2016.

[11] M. F. Córdoba-Erazo and T. M. Weller, "Noncontact Electrical Characterization of Printed Resistors Using Microwave Microscopy," *IEEE Transactions on Instrumentation and Measurement,* vol. 64, no. 2, pp. 509-515, 2015.

[12] "Silver Conductor CB028 Technical Datasheet," *Dupont,* 2013.

[13] M. K. Kim, J. Y. Hwang, H. Kang, K. Kang, S. H. Lee, and S. J. Moon, "Laser sintering of the printed silver ink," in *2009 IEEE International Symposium on Assembly and Manufacturing*, 2009, pp. 155-158.

[14] J. S. Hong and M. J. Lancaster, "Microstrip bandpass filter using degenerate modes of a novel meander loop resonator," *IEEE Microwave and Guided Wave Letters,* vol. 5, no. 11, pp. 371-372, 1995.

[15] E. A. Rojas-Nastrucci *et al.*, "Characterization and Modeling of K-Band Coplanar Waveguides Digitally Manufactured Using Pulsed Picosecond Laser Machining of Thick-Film Conductive Paste," *IEEE Transactions on Microwave Theory and Techniques,* vol. PP, no. 99, pp. 1-8, 2017.

[16] L. Ledezma and T. Weller, "Miniaturization of microstrip square open loop resonators using surface mount capacitors," in *WAMICON 2011 Conference Proceedings*, 2011, pp. 1-5.

[17] D. M. Pozar, "Microwave Engineering," (in English), 2012.

[18] M. Cordoba-Erazo, "Near-field Microwave Microscopy for Surface and Subsurface Characterization of Materials," *Dissertation, USF, Tampa, FL,* 2015.

[19] M. F. Córdoba-Erazo, E. A. Rojas-Nastrucci, and T. Weller, "Simultaneous RF electrical conductivity and topography mapping of smooth and rough conductive traces using microwave microscopy to identify localized variations," in *2015 IEEE 16th Annual Wireless and Microwave Technology Conference (WAMICON)*, 2015, pp. 1-4.

[20] J. Perelaer, M. Klokkenburg, C. E. Hendriks, and U. S. Schubert, "Microwave Flash Sintering of Inkjet-Printed Silver Tracks on Polymer Substrates," *Advanced Materials,* vol. 21, no. 47, pp. 4830-4834, 2009.

[21] J. Perelaer, B. J. de Gans, and U. S. Schubert, "Ink-jet Printing and Microwave Sintering of Conductive Silver Tracks," *Advanced Materials,* vol. 18, no. 16, pp. 2101-2104, 2006.

[22] H. Topsoe, "Geometric Factors in four point resistivity measurement," no. 472-13, p. 54, 1966.

Appendix A : Materials Characterization Using NFMM

In RF engineering quantifying the conductivity of our materials is of great importance. Having a high conductivity for metal traces and a high permittivity dielectric constant leads to lower loss in microstrip RF circuits. Typical methods of measuring DC conductivity include using a 4 point probe or Van der Pauw method, however while both methods allow for conductivity to be measured for homogenous bulk materials, it cannot be determined at the micro scale. Near Field Microwave Microscopy (NFMM) on the other hand does allow for measurements to be at the microscopic scale due to its small sized probe and ability to scan in microscopic steps which provide information that other methods cannot obtain. Measurements using the NFMM method can be used to determine values of conductivity near the surface of the sample. Bulk measurements such as using a four point probe and van der pauw on the other hand can be used to determine what the sheet resistance is in the bulk. Measurements using the 4 point probe assume that the material being measured is homogenous.

NFMM is an extensively used method to obtain the conductivity, relative permittivity, relative permeabilities of materials [11, 18, 19]. It is a non-contact technique that does not do damage to the material under test (MUT). This section describes the NFMM system that was used in order to obtain the measurements used in this work. The probe used for this work includes a dielectric resonator to measure the conductivity. It also employs a feedback system in order to monitor the correct height above the sample as well as a scanning mechanism which gives it the ability to scan across the surface to obtain a map of the surface and its material characteristics.

A.1 Dielectric Resonator Probe

The NFMM system used in imaging the conductivity employs a dielectric resonator (DR) operating at a resonance frequency of 5.73 GHz. A gold coated tungsten tip with a radius of 25 μm, is mounted to a RO4350B substrate with a dielectric resonator magnetically coupled across the 50 ohm microstrip lines enclosed in a metallic cavity shown in Figure A.1. When the tip is in midair the quality factor is ~1100. Several positioning systems are employed for movement in X, Y, and Z axes for macro alignment including three PI P-112.1DG stages with Mercury controllers. For micro-positioning a PI 611.ZS piezoelectric stage and E-816 controller are used.

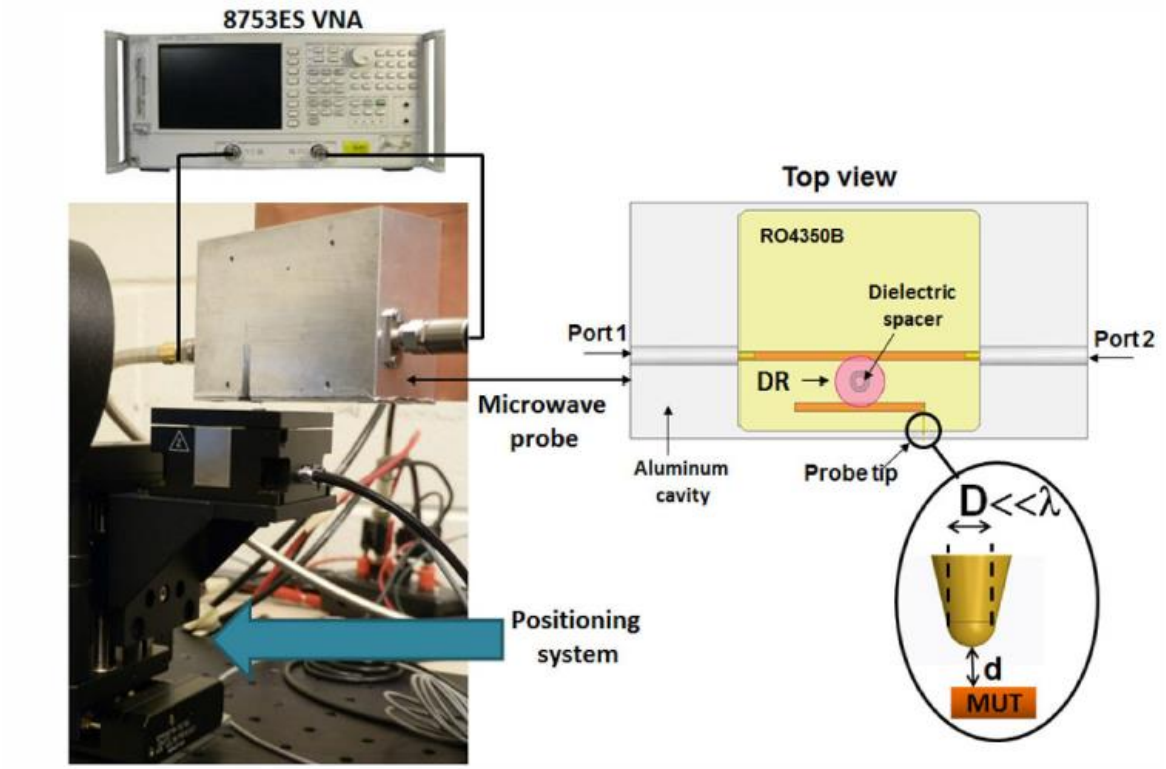

Figure A.1 NFMM system with dielectric resonator probe [19] © 2015 IEEE

The probe itself is sensitive to its surrounding environment. It has a different response when in midair compared to when it is direct contact with the MUT. Once the probe contacts the MUT the resonator shifts up in frequency as shown in Figure A.2b. A lumped element model of the probe near the MUT is shown in Figure A.2a.

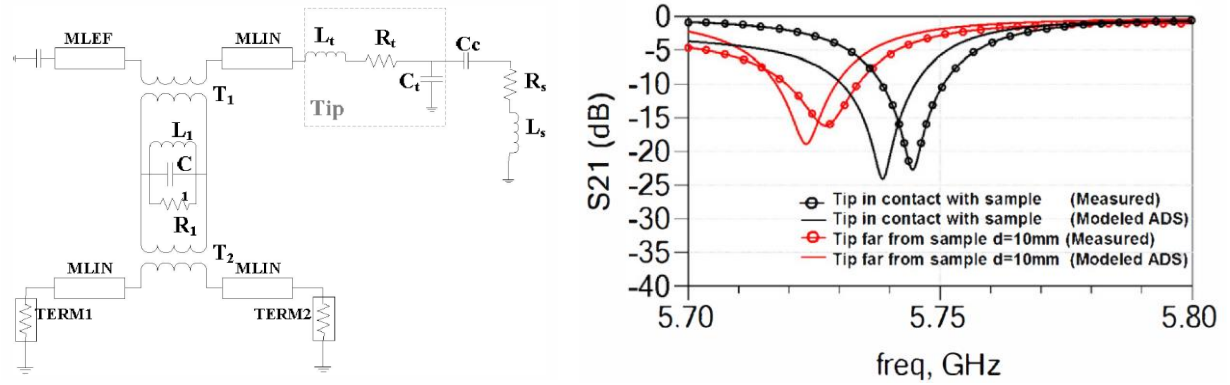

a) b)

Figure A.2 Lumped element model of a) Probe and sample, b) S21 of probe in contact with sample [19] © 2015 IEEE

Measurements on samples for this research were mounted on a 10 mm thick piece of ABS in order to help ensure that the resonator does not get too close to the metal motorized stages. The resonator is sensitive enough that surrounding metallic objects can affect the measurement of the Q. This helped to ensure that interferences from the surrounding environment were limited.

As the probe is lowered and approaches the surface of the MUT, both the resonance frequency and the quality factor decrease as shown in Figure A.3 and Figure A.4. The quality factor (Q) calculation is shown in Equations 11 and 12 and Figure A.3 [18]. The Q of the resonator is sensitive to the conductivity, and can be used in order to determine the value for unknown samples.

$$Q = \frac{1}{BW} = \frac{f_0}{f_3 - f_2} \tag{11}$$

$$x\,(dB) = 3 - 10\log(1 + 10^{-0.1L_{ins}}) \tag{12}$$

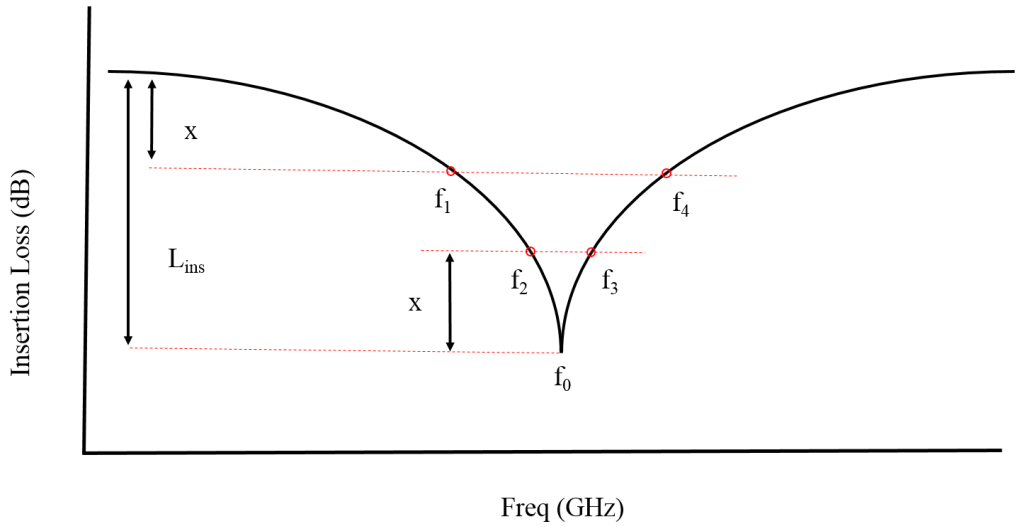

Figure A.3 Insertion loss versus frequency for a 2-port RLC resonator

By measuring the quality factor of known samples measured at a specific height **d** above the surface of the MUT**,** the conductivity of an unknown sample can be determined by using the data fit and measuring Q at the same height as the known samples shown in Figure 3.8. The known samples and their properties used to calibrate the probe in this research are shown in Table A.1.

Table A.1 Calibration material properties

Material	**Part Number**	**Size (mm3)**	**ρ (Ω*m)**	**σ (S/m)**
Ni	G1415	10x10x1	6.93E-08	1.44E+07
Ti	G140103	10x10x0.5	4.20E-07	2.38E+06
Stainless Steel	G14108	10x10x0.3	7.30E-07	1.37E+06

As the tip approaches the surface of the samples the Q value decreases depending upon the material. Figure A.4 shows the approach Q response for 3 calibration standards Nickel, Titanium, and Stainless Steel (SS). The VNA parameters used for this measurement are 0dB power with an IF BW of 1000 Hz, and a 6 scan average for each approach. The frequency response can also be seen in Figure A.5. As the tip approaches the surface only a sensitivity for Q can be seen with very little change in the resonance frequency (f_r).

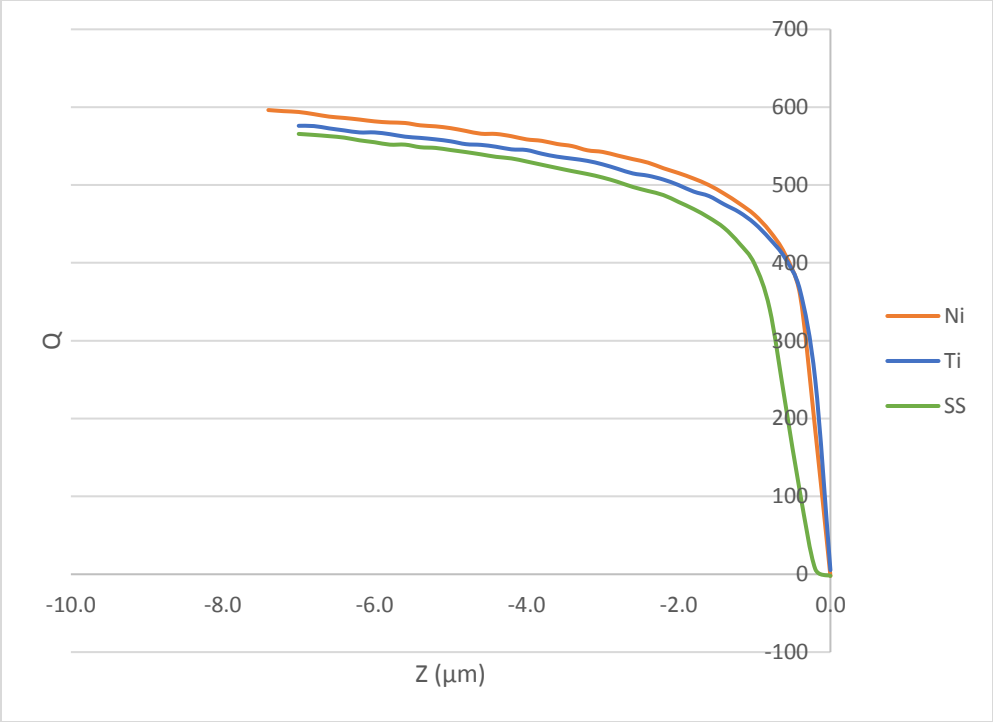

Figure A.4 NFMM response of Q during approach to calibration samples

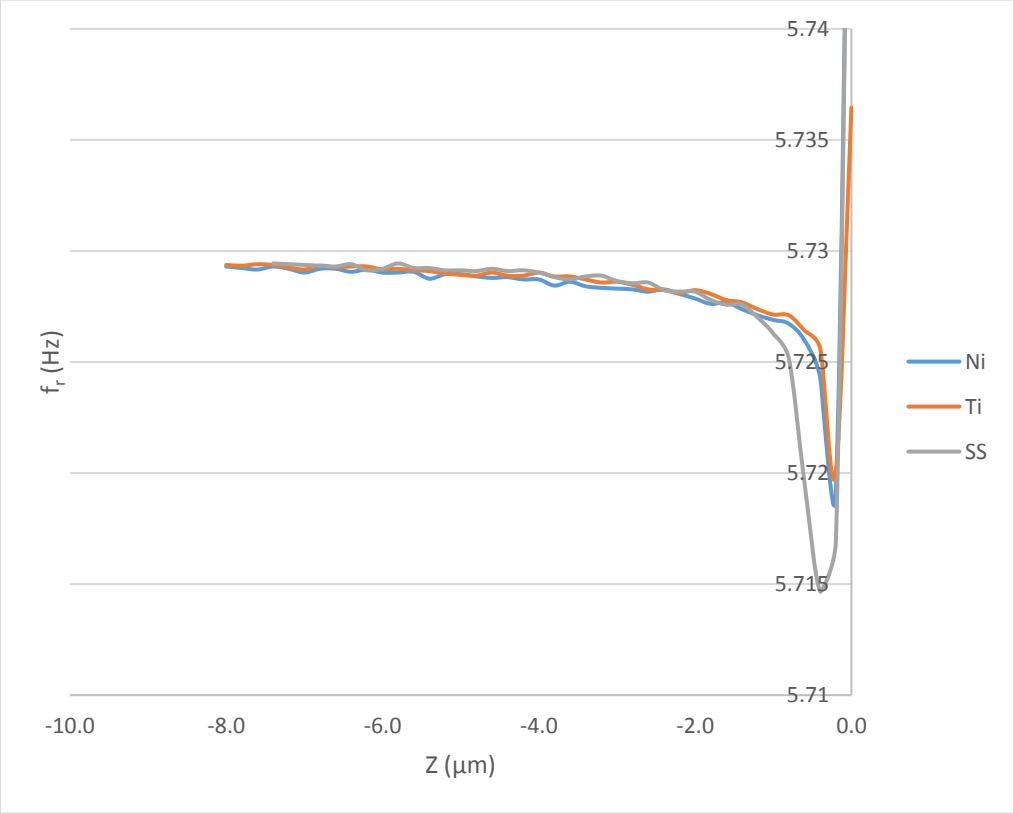

Figure A.5 NFMM response of f_r during approach to calibration samples

Calibration was preformed ensuring that the sample and the metallic calibration standard were measured at the exact same height. If an ink sample was measured on ABS then the calibration was performed on a piece of ABS that was at the exact same height as the ink sample. This helped to ensure that the probe during calibration was seeing the exact environment as the sample and helped to get a better calibration.

Appendix B : Microwaving Ink

One of the fundamental issues with 3D printing RF devices is the ink that is used in the printing process does not have a very high conductivity. The goal of this work was to improve the conductivity of the 3D printed silver ink by using a microwave to sinter the ink matrix in order to get better conductivity of the printed silver inks used in 3D printed RF devices. Described in this appendix are the experiments conducted in order to change the conductivity of the ink by microwaving, and the outcomes from the experiments.

B.1 Review of Previous Studies

When printing conductive inks onto 3D printed RF electronics the main goal is to get as high of conductivity as possible. There are a lot of different ways to print conductive traces onto surfaces as described in chapter 2 of this thesis. A typical method of curing the ink Dupont CB028 ink when printed and baked at 90° C for 60 minutes. This helps to ensure that the ink conductivity is as high as it can measures close to ~2.62 MS/m which is as high as we can get temperature wise since typical 3D printed parts are printed on ABS which has a very low melting temperature. It is important to try to develop new methods of improving the conductivity of the ink.

Several groups have previously studied the effects of microwaving ink in order to improve the inks electrical properties [20] [21]. Studies have been shown that the electrical properties can be improved with different exposure times.

B.2 Microwaving Test Experiments

Several squares of Dupont CB028 conductive ink were printed using an nScrypt 3Dn printer. Squares with the size of 10 cm x 10 cm were printed directly on top of ABS substrates with a thickness of 2 mm. The goal was to see the direct comparison of the conductivities of the ink that was oven baked followed by microwaving versus microwaving followed by baking. The baking was conducted at 90° C for 60 minutes, and the microwave power for all samples was 300W with varying microwaving times.

Experiment for set number 1 has the following steps:

1. Baked at 90°C for 1 hr
2. Microwaved

Experiment for set number 2 has the following steps:

1. Microwaved
2. Baked at 90°C for 1 hr

Figure B.1 and Table B.1 show that the samples that were baked prior to microwaving were found to have very little change in conductivity. Samples that were microwaved prior to being baked increased as they were microwaved longer periods of time with the power remaining the same. The conductivity of the samples were then obtained by using a Jandel RM3000 4 point probe taking an average of 4 measurements. A correction factor (G) was also multiplied by the sheet resistance in order to compensate for the geometry of the ink (10x10 mm) [22]. The G value used was 0.9313.

$$\sigma = \frac{1}{\rho} = \frac{1}{R_s * G * t} \tag{13}$$

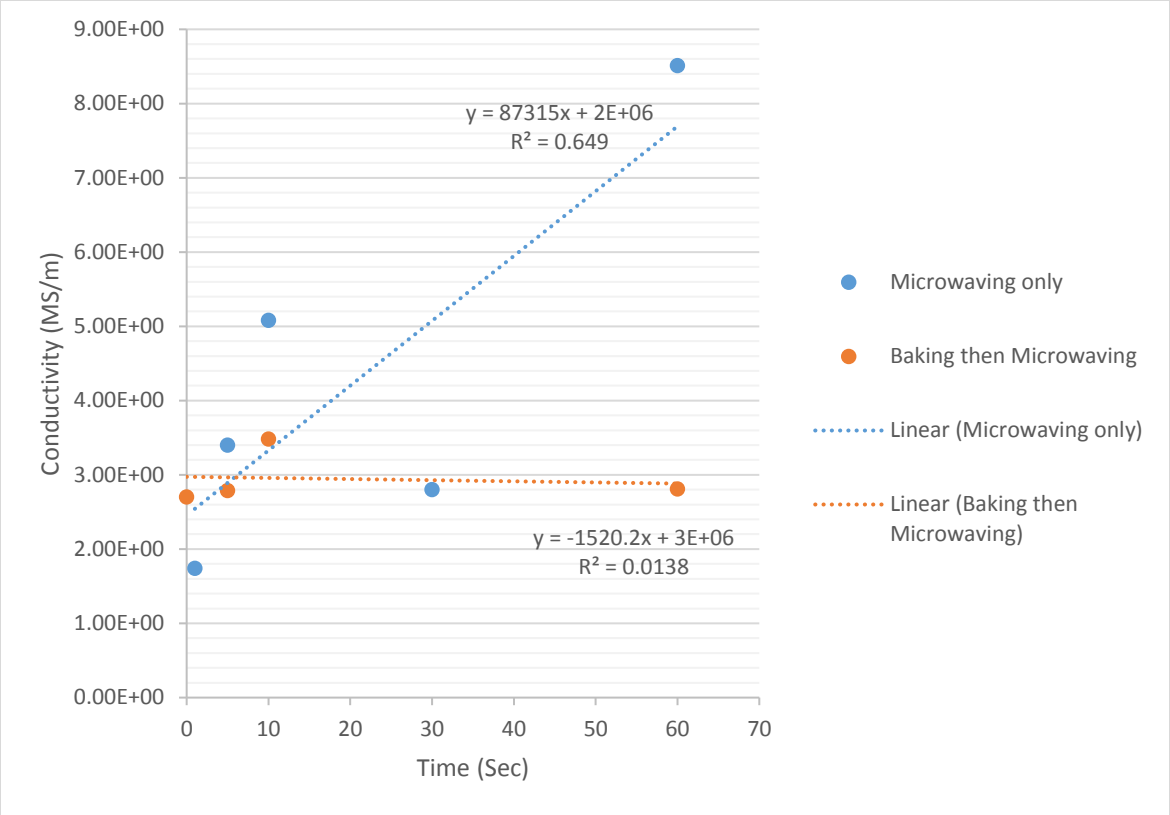

Figure B.1 Microwaving and baking conductivity comparison

Table B.1 Four probe conductivity measurements of microwaved ink

Microwaving followed by Baking			
Sample #	**Conductivity (S/m)**	**Time (sec)**	**Power (W)**
1	1.74E+06	1	300
5	3.40E+06	5	300
2	5.08E+06	10	300
4	2.80E+06	30	300
3	8.51E+06	60	300
Baking followed by Microwaving			
1	2.79e+06	5	300
2	3.48e+06	10	300
4	2.81e+06	60	300
5	2.70e+06	0	0

B.3 NFMM Measurements

NFMM measurements were also made in order to confirm a change in conductivity that was measured. Details describing the operation of the DR NFMM setup can be found in Appendix A. Scans were conducted on two of the samples that were microwaved prior to being oven baked at 1 second and 60 seconds, and the measured average Q was found to increase from 526 to 582 for the sample microwaved for 1 second and 60 seconds consecutively.

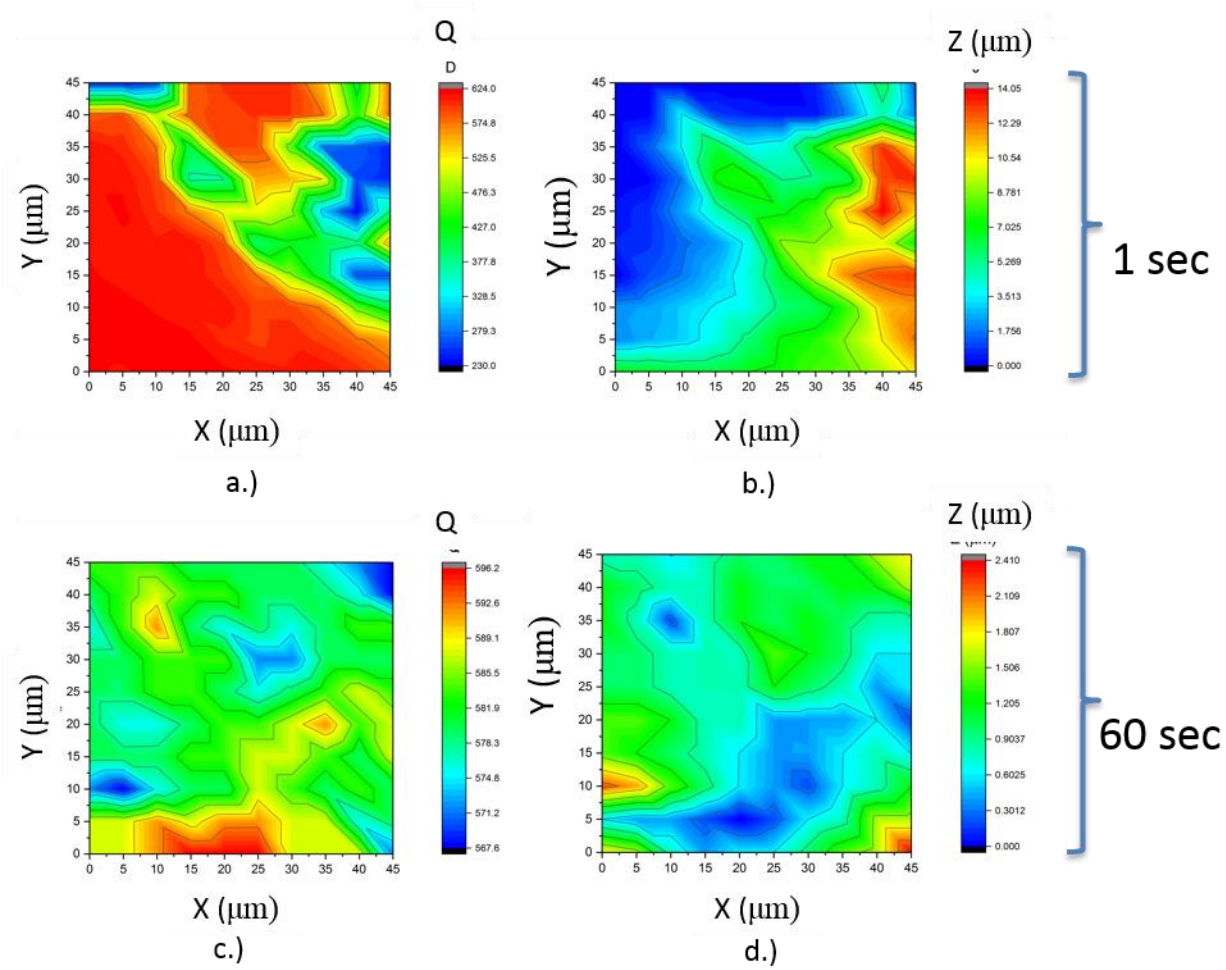

Figure B.2 NFMM images of microwaved ink surfaces a) Q for 1 sec b) Z for 1sec c) Q for 60 sec d) Z for 60 sec

It is important to note that when the average Q values measured using the NFMM are matched up with values shown on the calibration curve shown in Figure 3.8, they are consistent with each other. The σ values that were measured with the 4 point probe shown below in Table B.2.

Table B.2 Comparison of σ between 4 point probe and NFMM

Time (sec)	σ (S/m) with 4 probe	NFMM Q	σ (S/m) with NFMM
1	1.74E+06	526	~4E+06
60	8.51E+06	582	~12E+06

Appendix C : Additional NFMM Scanned Data

One map of conductivity using the NFMM shows a max conductivity of 32 MS/m near the edge of the gap. This NFMM map was imaged across a 16 μm gap laser machined SOLR resonator. The radius of the tip of the NFMM is 25 μm, so it was difficult to obtain the image of the gap itself. It does however show that the conductivity could be higher in regions. In previous work the extracted effective conductivity of the ink for a laser machined resonator is 32.27 MS/m, and filter is 17.5 MS/m [15]. This measurement shows that samples have higher values of conductivity near the edge that are closer to the previously determined values.

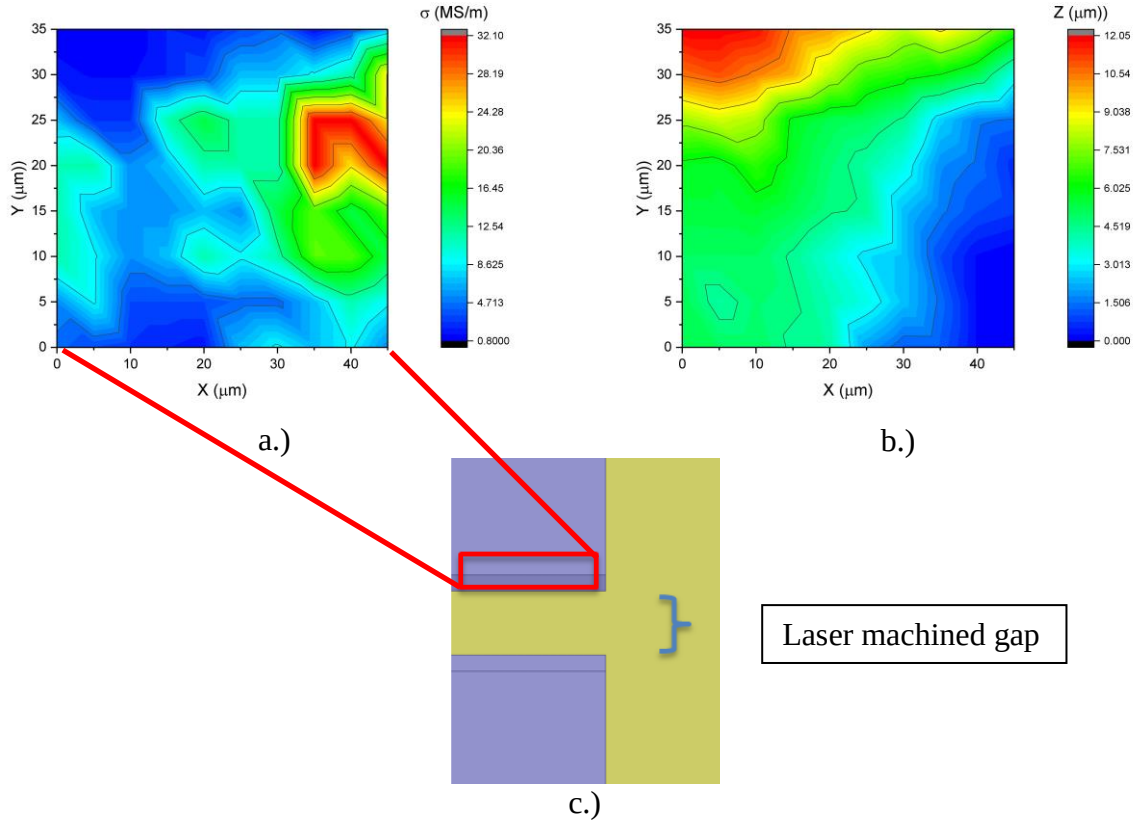

Figure C.1 NFMM map of near the laser machined gap

Appendix D : Copyright Permissions

The permission from IEEE to use Figure 2.1 and Figure 2.4 is below.

Copyright Clearance Center RightsLink®

Home | Create Account | Help

IEEE Requesting permission to reuse content from an IEEE publication

Title: Multimaterial and Multilayer Direct Digital Manufacturing of 3-D Structural Microwave Electronics
Author: Kenneth H. Church
Publication: Proceedings of the IEEE
Publisher: IEEE
Date: April 2017
Copyright © 2017, IEEE

LOGIN
If you're a copyright.com user, you can login to RightsLink using your copyright.com credentials. Already a RightsLink user or want to learn more?

Thesis / Dissertation Reuse

The IEEE does not require individuals working on a thesis to obtain a formal reuse license, however, you may print out this statement to be used as a permission grant:

Requirements to be followed when using any portion (e.g., figure, graph, table, or textual material) of an IEEE copyrighted paper in a thesis:

1) In the case of textual material (e.g., using short quotes or referring to the work within these papers) users must give full credit to the original source (author, paper, publication) followed by the IEEE copyright line © 2011 IEEE.
2) In the case of illustrations or tabular material, we require that the copyright line © [Year of original publication] IEEE appear prominently with each reprinted figure and/or table.
3) If a substantial portion of the original paper is to be used, and if you are not the senior author, also obtain the senior author's approval.

Requirements to be followed when using an entire IEEE copyrighted paper in a thesis:

1) The following IEEE copyright/ credit notice should be placed prominently in the references: © [year of original publication] IEEE. Reprinted, with permission, from [author names, paper title, IEEE publication title, and month/year of publication]
2) Only the accepted version of an IEEE copyrighted paper can be used when posting the paper or your thesis on-line.
3) In placing the thesis on the author's university website, please display the following message in a prominent place on the website: In reference to IEEE copyrighted material which is used with permission in this thesis, the IEEE does not endorse any of [university/educational entity's name goes here]'s products or services. Internal or personal use of this material is permitted. If interested in reprinting/republishing IEEE copyrighted material for advertising or promotional purposes or for creating new collective works for resale or redistribution, please go to http://www.ieee.org/publications_standards/publications/rights/rights_link.html to learn how to obtain a License from RightsLink.

If applicable, University Microfilms and/or ProQuest Library, or the Archives of Canada may supply single copies of the dissertation.

BACK | CLOSE WINDOW

The permission from IEEE to use Table 2.1 and Table 2.2 is below.

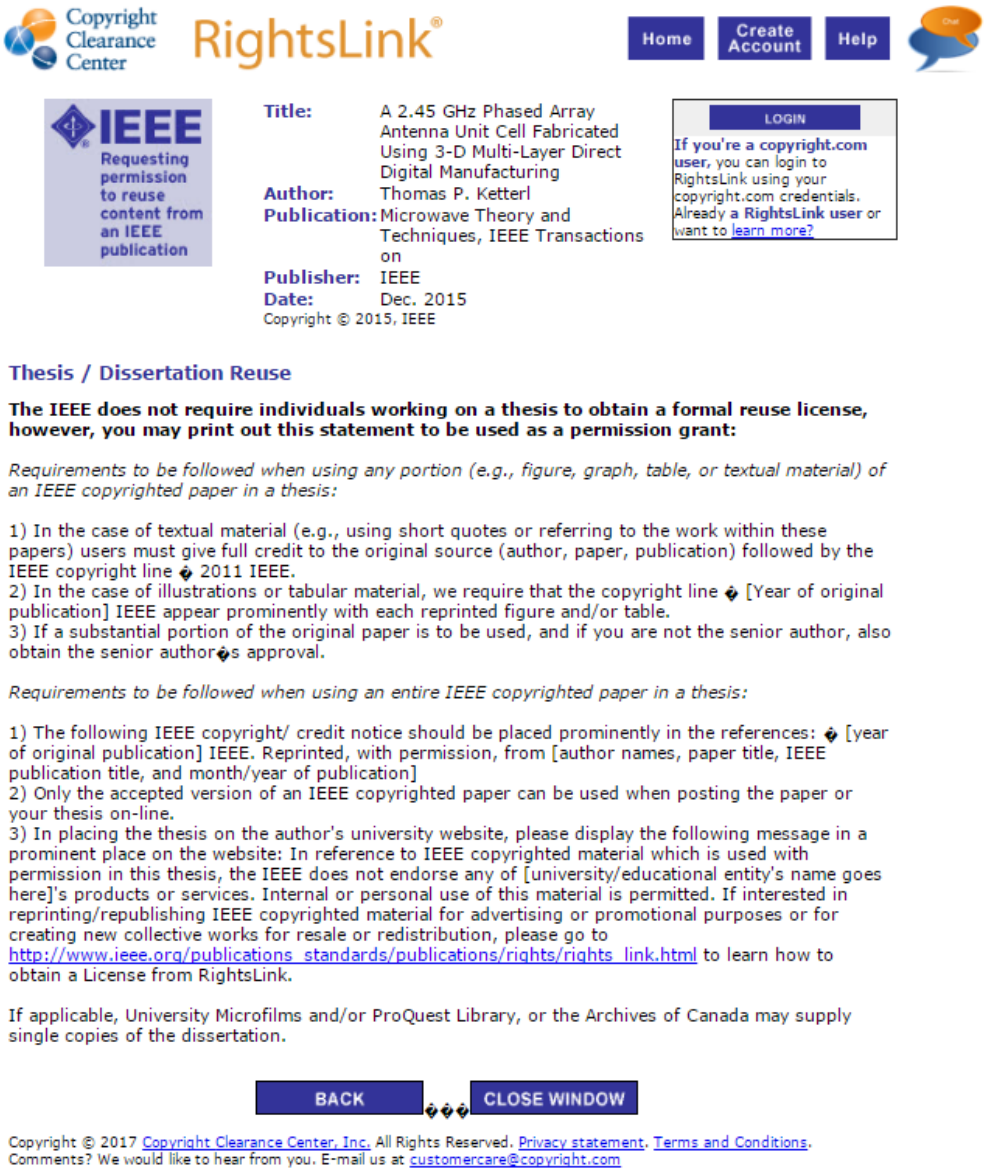

Copyright Clearance Center RightsLink®

Home | Create Account | Help

IEEE Requesting permission to reuse content from an IEEE publication

Title: A 2.45 GHz Phased Array Antenna Unit Cell Fabricated Using 3-D Multi-Layer Direct Digital Manufacturing
Author: Thomas P. Ketterl
Publication: Microwave Theory and Techniques, IEEE Transactions on
Publisher: IEEE
Date: Dec. 2015
Copyright © 2015, IEEE

LOGIN
If you're a copyright.com user, you can login to RightsLink using your copyright.com credentials. Already a RightsLink user or want to learn more?

Thesis / Dissertation Reuse

The IEEE does not require individuals working on a thesis to obtain a formal reuse license, however, you may print out this statement to be used as a permission grant:

Requirements to be followed when using any portion (e.g., figure, graph, table, or textual material) of an IEEE copyrighted paper in a thesis:

1) In the case of textual material (e.g., using short quotes or referring to the work within these papers) users must give full credit to the original source (author, paper, publication) followed by the IEEE copyright line © 2011 IEEE.
2) In the case of illustrations or tabular material, we require that the copyright line © [Year of original publication] IEEE appear prominently with each reprinted figure and/or table.
3) If a substantial portion of the original paper is to be used, and if you are not the senior author, also obtain the senior author's approval.

Requirements to be followed when using an entire IEEE copyrighted paper in a thesis:

1) The following IEEE copyright/ credit notice should be placed prominently in the references: © [year of original publication] IEEE. Reprinted, with permission, from [author names, paper title, IEEE publication title, and month/year of publication]
2) Only the accepted version of an IEEE copyrighted paper can be used when posting the paper or your thesis on-line.
3) In placing the thesis on the author's university website, please display the following message in a prominent place on the website: In reference to IEEE copyrighted material which is used with permission in this thesis, the IEEE does not endorse any of [university/educational entity's name goes here]'s products or services. Internal or personal use of this material is permitted. If interested in reprinting/republishing IEEE copyrighted material for advertising or promotional purposes or for creating new collective works for resale or redistribution, please go to http://www.ieee.org/publications_standards/publications/rights/rights_link.html to learn how to obtain a License from RightsLink.

If applicable, University Microfilms and/or ProQuest Library, or the Archives of Canada may supply single copies of the dissertation.

BACK | CLOSE WINDOW

Copyright © 2017 Copyright Clearance Center, Inc. All Rights Reserved. Privacy statement. Terms and Conditions.
Comments? We would like to hear from you. E-mail us at customercare@copyright.com

The permission from IEEE to use Figure 2.2 is below.

Copyright Clearance Center RightsLink®

Home | Create Account | Help

IEEE Requesting permission to reuse content from an IEEE publication

Title: Infill-Dependent 3-D-Printed Material Based on NinjaFlex Filament for Antenna Applications
Author: Stefano Moscato
Publication: IEEE Antennas and Wireless Propagation Letters
Publisher: IEEE
Date: 2016
Copyright © 2016, IEEE

LOGIN
If you're a copyright.com user, you can login to RightsLink using your copyright.com credentials. Already a RightsLink user or want to learn more?

Thesis / Dissertation Reuse

The IEEE does not require individuals working on a thesis to obtain a formal reuse license, however, you may print out this statement to be used as a permission grant:

Requirements to be followed when using any portion (e.g., figure, graph, table, or textual material) of an IEEE copyrighted paper in a thesis:

1) In the case of textual material (e.g., using short quotes or referring to the work within these papers) users must give full credit to the original source (author, paper, publication) followed by the IEEE copyright line © 2011 IEEE.
2) In the case of illustrations or tabular material, we require that the copyright line © [Year of original publication] IEEE appear prominently with each reprinted figure and/or table.
3) If a substantial portion of the original paper is to be used, and if you are not the senior author, also obtain the senior author's approval.

Requirements to be followed when using an entire IEEE copyrighted paper in a thesis:

1) The following IEEE copyright/ credit notice should be placed prominently in the references: © [year of original publication] IEEE. Reprinted, with permission, from [author names, paper title, IEEE publication title, and month/year of publication]
2) Only the accepted version of an IEEE copyrighted paper can be used when posting the paper or your thesis on-line.
3) In placing the thesis on the author's university website, please display the following message in a prominent place on the website: In reference to IEEE copyrighted material which is used with permission in this thesis, the IEEE does not endorse any of [university/educational entity's name goes here]'s products or services. Internal or personal use of this material is permitted. If interested in reprinting/republishing IEEE copyrighted material for advertising or promotional purposes or for creating new collective works for resale or redistribution, please go to http://www.ieee.org/publications_standards/publications/rights/rights_link.html to learn how to obtain a License from RightsLink.

If applicable, University Microfilms and/or ProQuest Library, or the Archives of Canada may supply single copies of the dissertation.

BACK | CLOSE WINDOW

Copyright © 2017 Copyright Clearance Center, Inc. All Rights Reserved. Privacy statement. Terms and Conditions.
Comments? We would like to hear from you. E-mail us at customercare@copyright.com

The permission from IEEE to use image in Figure 3.2 is below.

Title: Characterization and Modeling of K-Band Coplanar Waveguides Digitally Manufactured Using Pulsed Picosecond Laser Machining of Thick-Film Conductive Paste
Author: Eduardo A. Rojas-Nastrucci
Publication: Microwave Theory and Techniques, IEEE Transactions on
Publisher: IEEE
Date: Dec 31, 1969
Copyright © 1969, IEEE

LOGIN

If you're a copyright.com user, you can login to RightsLink using your copyright.com credentials. Already a RightsLink user or want to learn more?

Thesis / Dissertation Reuse

The IEEE does not require individuals working on a thesis to obtain a formal reuse license, however, you may print out this statement to be used as a permission grant:

Requirements to be followed when using any portion (e.g., figure, graph, table, or textual material) of an IEEE copyrighted paper in a thesis:

1) In the case of textual material (e.g., using short quotes or referring to the work within these papers) users must give full credit to the original source (author, paper, publication) followed by the IEEE copyright line © 2011 IEEE.
2) In the case of illustrations or tabular material, we require that the copyright line © [Year of original publication] IEEE appear prominently with each reprinted figure and/or table.
3) If a substantial portion of the original paper is to be used, and if you are not the senior author, also obtain the senior author's approval.

Requirements to be followed when using an entire IEEE copyrighted paper in a thesis:

1) The following IEEE copyright/ credit notice should be placed prominently in the references: © [year of original publication] IEEE. Reprinted, with permission, from [author names, paper title, IEEE publication title, and month/year of publication]
2) Only the accepted version of an IEEE copyrighted paper can be used when posting the paper or your thesis on-line.
3) In placing the thesis on the author's university website, please display the following message in a prominent place on the website: In reference to IEEE copyrighted material which is used with permission in this thesis, the IEEE does not endorse any of [university/educational entity's name goes here]'s products or services. Internal or personal use of this material is permitted. If interested in reprinting/republishing IEEE copyrighted material for advertising or promotional purposes or for creating new collective works for resale or redistribution, please go to http://www.ieee.org/publications_standards/publications/rights/rights_link.html to learn how to obtain a License from RightsLink.

If applicable, University Microfilms and/or ProQuest Library, or the Archives of Canada may supply single copies of the dissertation.

BACK CLOSE WINDOW

The permissions from IEEE to use Figure A.1 and Figure A.2 is below.